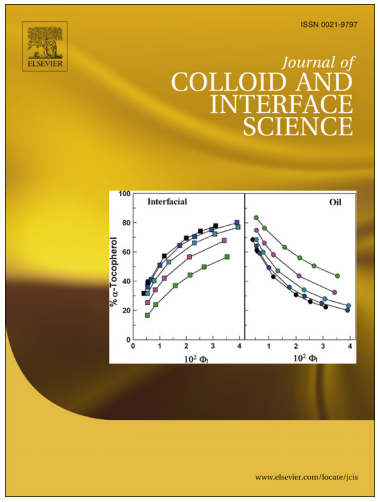

Polyoxometalate-grafted graphene nanohybrid for electrochemical detection of hydrogen peroxide and glucose

MinHo Yang, Dong Seok Kim, Tae Jae Lee, Seok Jae Lee, Kyoung G. Lee, Bong Gill Choi

PII: S0021-9797(16)30047-9
DOI: http://dx.doi.org/10.1016/j.jcis.2016.01.047
Reference: YJCIS 21030

To appear in: *Journal of Colloid and Interface Science*

Received Date: 16 December 2015
Revised Date: 18 January 2016
Accepted Date: 20 January 2016

Please cite this article as: M. Yang, D.S. Kim, T.J. Lee, S.J. Lee, K.G. Lee, B.G. Choi, Polyoxometalate-grafted graphene nanohybrid for electrochemical detection of hydrogen peroxide and glucose, *Journal of Colloid and Interface Science* (2016), doi: http://dx.doi.org/10.1016/j.jcis.2016.01.047

Polyoxometalate-grafted graphene nanohybrid for electrochemical detection of hydrogen peroxide and glucose

MinHo Yang,[†] Dong Seok Kim,[‡] Tae Jae Lee,[†] Seok Jae Lee[†], Kyoung G. Lee,[†,*] and Bong Gill Choi[‡,*]

[†]Department of Nano Bio Research, National NanoFab Center (NNFC), Daejeon 34141, Republic of Korea

[‡]Department of Chemical Engineering, Kangwon National University, Samcheok 25913, Republic of Korea

*Co-Corresponding author.
E-mail: kglee@nnfc.re.kr (K. G. Lee)

*Co-Corresponding author.
E-mail: bgchoi@kangwon.ac.kr (B. G. Choi)
Fax: +82-33-570-6535
Tel: +82-33-570-6545

Abstract

The electrochemical performances of electrochemical biosensors largely depend on electrode characteristics, such as size, composition, surface area, and electron and ion conductivities. Herein, highly efficient electrocatalytic polyoxometalate (POM) was directly deposited on polymeric ionic liquid (PIL)-functionalized reduced graphene oxide (rGO) in a simple manner. The nano-sized POM with PIL functional groups was uniformly distributed on the surface of rGO sheets. The unique nanostructure of the resultant POM-g-rGO nanohybrids enabled well-defined multiple redox reaction of POMs and rapid electron transfer. In particular, as-prepared nanohybrids demonstrated high electrocatalytic activity for the electrochemical detection of H_2O_2 and glucose molecules in flow-injection biosensor device with high sensitivity, rapid response time, and low detection limit.

Keywords: Polyoxometalate, Graphene, Nanohybrid, Ionic liquid, Electrochemical sensor

1. Introduction

Nanostructured materials have been extensively employed to prepare an electrode for electrochemical devices due to their large surface areas, high mass transport rate, and excellent electrocatalytic properties [1,2]. Recently, the integration of conductive carbon materials and metal (or metal oxide) nanoparticles is of great interest in the material science and practical applications [3–6]. Such nanohybrid materials provide great opportunities for the fine tuning multiple functionalities [7]. In particular, nanoparticles anchored on graphene sheets are one of the most widely used nanohybrid materials for electrochemical biosensor applications targeting hydrogen peroxide, NADH, ascorbic acid, dopamine, and others [8−12]. Graphene acts as an excellent support on which to deposite nanoparticles and a conducting pathway to assist a fast electrochemical kinetics during electrocatalytic reactions [13]. On the other hand, of the various electrocatalytic nanoparticles, polyoxometalates (POMs) are considered as versatile nano-building blocks for the construction of nanohybrid materials due to their multiple charge transfer reactions and unique structural, electronic, and optical properties [14]. POM-based nanohybrid materials are particularly effective electrochemical catalysts in the detection of nitrate, iodate, bromate, and H_2O_2 [15−18]. Owing to this electrocatalytic effect of POMs toward reduction of H_2O_2, POM-based nanohybrid materials are also suitable for use in electrochemical glucose biosensors. Despite these attractive features of POMs, high solubility of POMs in aqueous solution limit their direct use in electrochemical systems [19], and thus, main strategy is to prepare POM-based nanohybrid materials.

Herein, we describe the electrocatalytic characteristics of a POM-grafted reduced graphene oxide (POM-g-rGO) nanohybrid for development of electrochemical sensors for detection of H_2O_2 and glucose molecules. In preparation of POM-g-rGO nanohybrids, a polymeric ionic

liquid (PIL) was employed to link POMs to rGO. This process not only prevents rGO sheet aggregation, which commonly occurs during the reduction of GO sheets, but also facilitates charge transfer at the electrode/electrolyte interface. The electrochemical sensing performances of POM-g-rGO nanohybrids were thoroughly examined by incorporating them as electrodes in a injection-flow system. The POM-g-rGO nanohybrids showed high electrocatalytic activities toward H_2O_2 and glucose with high sensitivity, low detection limit, and rapid response time.

2. Material and methods

2.1. Materials

All chemicals were used a received without further purification. The GO was synthesized from natural graphite (Sigma Aldrich, <20 μm) using a modified Hummers methods [20]. The rGO was prepared by the chemical reduction of GO using hydrazine hydrate. The PIL, poly(1-vinyl-3-ethylimidazolium bromide), was prepared according to previously reported procedure [21]. Hydrazine monohydrate (64 – 65%), phosphomolybdic acid hydrate ($H_3[PMo_{12}O_{40}]\cdot xH_2O$, denoted by POM), potassium hexacyanoferate (III) ($K_3Fe(CN)_6$), and potassium hexacyanoferate (II) trihydrate ($K_4Fe(CN)_6\cdot 3H_2O$), glucose oxidase (GOx, EC1.1.3.4, from *Aspergillus niger*, ~200 U/mg), β-D-(+)-glucose, ascorbic acid (AA), and uric acid (UA) were obtained from Sigma-Aldrich. Hydrogen peroxide (H_2O_2, 30% w/w) was purchased from Junsei.

2.2. Preparation of the POM-g-rGO Nanocomposites

To prepare POM-g-rGO, aqueous a PIL-GO suspension was prepared by mixing GO (5 mg) with PIL (10 mg) in 20 mL of deionized (DI) water. Chemical reduction of GO was conducted by adding 20 μL of hydrazine monohydrate and heating at 85 °C for 24 h. The stable black-colored PIL-rGO suspension obtained was filtered through an Anodisc membrane filter (pore

size 0.20 μm, Whatman) and washed extensively with DI water to remove any residual hydrazine and unbound PIL. After drying under ambient conditions, the PIL-rGO was re-dispersed in DI water and mixed with excess POM. The resulting suspension was vigorously stirred overnight to yield POM-g-rGO by anion exchange. Finally, POM-g-rGO was collected by filtration and thoroughly washed with DI water to remove any unbound POM.

2.3. Preparation of nanohybrid-modified electrode and immobilization of GOx

Before surface modification, glassy carbon electrode (GCE, dia 3 mm) was polished with 0.05 μm alumina sequentially, rinsed with DI water, sonicated in water bath and dried in air. Then, 5 mg of POM-g-rGO was first suspended in 10 mL of DI water and sonicated for 1 h. Next, a 5 μL of POM-g-rGO suspension was dropped onto the surface of GCE. After drying in air, an aliquot of 5 μL Nafion solution (1 wt% in propanol) was casted on the layer of POM-g-rGO in order to entrap POM-g-rGO. The as-prepared electrode was immersed in DI water for 1 h to wet the Nafion layer thoroughly before use. For immobilization of GOx, 6 μL of 3 mg/mL GOx was dropped on the surface of the POM-g-rGO electrode. A 5 μL Nafion solution was dropped on the enzyme electrode (GOx/POM-g-RGO) and dried for 24 h at 4 °C to form a uniform structure. After drying, the prepared enzyme electrode was washed with copious PBS to remove the non-immobilized GOx.

2.4. Fabrication of microfluidic electrochemical sensor

Microfluidic sensor was fabricated by integrating a fluidic channel substrate with POM-g-rGO or GOx/POM-g-RGO nanohybrids. The microfluidic device was based on plastic substrates with an oval-shaped flow channel. The device was equipped with two holes of inlet and outlet, an Ag/AgCl reference electrode, and a Pt counter electrode. A syringe pump (KD scientific, KDS 100) and injection valve (Rhoedyne, model 7725i) with a HPLC-grade sample loop was used to

pump the carrier solution (20 μL) and to inject H_2O_2 and glucose for the microfluidic detection system, respectively.

2.5. Characterization

Transmission electron microscopy (TEM) images were obtained using a field-emission TEM (JEM2100F, JEOL Ltd.) operated at 200 kV. Scanning electron microscopy (SEM) images were obtained using a field emission scanning electron microscope (S-4800, Hitachi). X-ray photoelectron spectroscopy (XPS) data were obtained using a Thermo MultiLab 2000 system. An Al MgαX-ray source at 200 W was used with pass energy of 20 eV and a 45° takeoff angle in a 10^{-7} Torr vacuum analysis chamber. All electrochemical measurements were performed on a CHI 760E electrochemical workstation (CH Instruments) using a conventional three-electrode system. Flow injection mode in microfluidic sensor was performed with chronoamperometric technique. All flow injection measurements were carried out at a flow rate of 1 mL/min. All potentials were collected at room temperature, and the as-obtained data were within the error range of ±1%.

3. Results and Discussion

Figure 1a displays typical photographs of rGO and POM-g-rGO dispersed in aqueous solution. The rGO was not dispersed in water, but the POM-g-rGO was well dispersed in water, because of its abundant hydrophilic anionic sites of POMs. In addition, the imidazolitum cations of PIL were interacted with rGO sheets through cation–π interaction, while Br^- anions of PIL were exchanged with POMs through anion exchange reaction [21]. To investigate the colloidal stabilities of rGO, PIL-rGO and POM-g-rGO, we measured zeta potentials and found them to be −10.47 mV for rGO, indicating instability of rGO colloidal suspension. The zeta potential values of PIL-rGO and POM-g-rGO had +34.70 mV and −38.05 mV, respectively, indicating well-dispersed colloidal suspensions [22]. The opposite and negative zeta potentials of PIL-rGO and POM-g-rGO suggest different surface charges on adsorbed PIL (positive charge) and POM (negative charge) molecules on the graphene surface. As shown in Figure 1b, TEM image of the POM-g-rGO nanohybrid revealed ultra-thin crumpled nanosheets of rGOs, in which nano-sized POM particles were uniformly distributed. Elemental mapping confirmed the nanohybrid structure of POM-g-rGO. Strong signals for molybdenum for POM, carbon for rGO, and nitrogen for PIL were simultaneously observed at the surface of POM-g-rGO, indicating co-existence of POM, PIL, and rGO. XPS was employed to investigate variations in elemental composition and functional groups in samples. Figure 2a shows the survey XPS spectra of PIL-rGO and POM-g-rGO samples. Compared to the bare PIL-rGO sample, a Mo peak appeared at the POM-g-rGO nanohybrid due to successful exchange between PIL counter anion and POM. The C 1s XPS spectrum of POM-g-rGO is deconvoluted into the four peaks corresponding to carbon atoms in different functional groups (Figure 2b). The peak centered at 248.5 eV was attributed to C–C/C=C bonds. The other peaks at 285.93, 286.76, and 288.06 eV were assigned

to C–N, C–O, and C=O bonds, respectively. The C–C/C=C group countent in POM-g-rGO was calculated to be ~71%, which is much higher than that of previously reported for GO [23,24]. These results reveal the successful attachment of PIL and reduction of GO by hydrazine. Mo 3d XPS data exhibited two dominant peaks centered at 232.37 and 235.53 eV, which were assigned to fully oxidized Mo^{6+} in the form of MoO_3 (Figure 2c). In addition, binding energies at 230.94 and 234.27 eV were assigned to partially oxidized Mo^{5+} (230.94 and 234.27 eV), resulting from the attachment of POM to PIL-rGO sheets and charge transfer between PIL-rGO to the LUMO of the POM cluster [25]. The O 1s spectrum in Figure 2d shows peaks at 530.68 and 532.62 eV corresponding to the oxygen in $PMo_{12}O_{40}^{3-}$ and to chemisorbed water or to other hydroxide groups attached to metal centers, respectively.

To investigate the electrochemical behavior of the POM-g-rGO nanohybrid, CV measurements were conducted using a three electrode system consisting of a working electrode of PIL-g-rGO, a counter electrode of Pt wire, and a reference electrode of Ag/AgCl electrode. The electrolyte was 0.5 M H_2SO_4. As shown in Figure 3a, we found clear multiple reversible redox peaks in POM-g-rGO compared to the POM-rGO and PIL-rGO. In addition, the peak-to-peak separations between anodic and cathodic peaks (ΔE_p) of POM-g-rGO are smaller than that of POM-rGO. This behavior was attributed to introduction of ILs in nanohybrids leading to efficient immobilization of POMs and facilitated the electron transfer between POM and rGO.

CV measurements were also performed at different scan rates ranging from 10 to 1000 mV/s (Figure 3b). The POM-g-rGO nanohybrid showed an increased current response on increasing the scan rate and exhibited three pairs of well-defined redox peaks. This is attributed to efficient and rapid charge transfer between POMs and rGOs. We plotted the second oxidation peak as a function of scan rate (Inset in Figure 3b). A linear relationship was found between anodic peak currents and scan rates (R^2 = 0.9986 and 0.9995 for anodic and cathodic peaks, respectively).

This finding indicates that the redox reaction of POMs on the surface of rGO was governed by a surface confined redox process [26].

The electrocatalytic reduction of H_2O_2 on POM-g-rGO was evaluated by a flow-injection amperometry. In order to obtain on-set potential for amperometric measurements, CV measurements were conducted in presence and absence of 10 mM H_2O_2 (Figure 4). The mechanism of electrocatalytic reduction of H_2O_2 was as follows [27]:

$$H_2O_2 + e^- \rightarrow OH_{ad} + OH^-$$

$$OH_{ad} + e^- \rightarrow OH^-$$

$$2OH^- + 2H^+ \rightarrow 2H_2O$$

Obviously, the POM-g-rGO nanohybrid exhibited an increase in cathodic reduction peak when H_2O_2 was introduced. This indicates a high electrocatalytic ability of POMs in POM-g-rGO. The flow-injection system used for the electrochemical detection of H_2O_2 was operated at an on-set potential of +0.02 V using a three electrode system (Figure 5). The amperometric response of the POM-g-rGO electrode was followed with the successive addition of H_2O_2. The reduction current increased constantly on increasing H_2O_2 concentration. All of the cathodic current appeared within ~ 5 s, which is indicative of a fast response time of POM-g-rGO. These current signals were plotted as a function of H_2O_2 concentration. The sensing performance of the POM-g-rGO had a wide detection range of H_2O_2 detection (100 μM – 20 mM). In particular, the POM-g-rGO had as high as sensitivity of 95.5 $\mu A/mM \cdot cm^2$, which is higher than those of other electrocatalytic materials, including nanoporous PtCu (13.61 $\mu A/mM \cdot cm^2$), MnO_2/GO (38.2 $\mu A/mM \cdot cm^2$), and Ag-MnO_2-MWNTs (82.5 $\mu A/mM \cdot cm^2$) nanocomposites [28–30]. Using the noise level and the relationship between current response and H_2O_2 concentration (S/N = 3), the POM-g-rGO showed a very low limit of detection (LOD) of 10.2 μM.

Electrochemical biosensors for detection of glucose are now utilized in portable units for the monitoring and management of diabetes because these biosensors are easily used, and provide rapid and accurate measurements [31]. In typical enzymatic glucose sensors, the electrode measured H_2O_2 molecules generated from the oxidation reaction of glucose by GOx as the following reactions [31]:

$$GOx–FADH_2 + O_2 \rightarrow GOx–FAD + H_2O_2$$

$$H_2O_2 \rightarrow O_2 + 2H^+ + 2e^-$$

The electrochemical performance of the glucose sensor based on the GOx/POM-g-rGO nanohybrid was evaluated in a flow-injection system using chronoamperometric measurements. Current response was determined at an applied on-set potential of +0.02 V at glucose concentrations increased incrementally from 2 to 20 mM. As concentration increased, maximum current signals increased constantly. All current signals were detected within ~ 5 s and subsequently returned to baseline, indicating a rapid response time of glucose biosensor. The response currents obtained at different glucose concentration were plotted in Figure 6a, which showed a well-defined linear relationship (current signal *vs.* glucose concentration). Based on the slope of calibration plots, the corresponding sensitivity was estimated to be 14.3 $\mu A/mM \cdot cm^2$. The detection range for glucose from 2 to 20 mM as determined in this study is enough for detection in real sample of glucose [31]. In addition, the LOD was calculated to be as low as 67.9 μM, which is much lower than other reported POM-based electrode for glucose [32]. In order to investigate selectivity for glucose, the GOx/POM-g-rGO was tested in the presence of AA and UA, which are considered interfering species. At an applied polarization potential of +0.02 V, AA (0.2 mM) and UA (0.2 mM) produced negligible signals (Figure 6b). In contrast, a strong current signal was observed after injecting glucose (2 mM). Furthermore, this current was also

observed after injecting a mixture of glucose (2 mM), AA (0.2 mM), and UA (0.2 mM). This data clearly demonstrates that the GOx/POM-g-rGO electrode has good selectivity performance for glucose from the main interfering species in real blood.

Conclusion

We suggested a straightforward method for preparation of highly efficient electrocatalytic nanohybird of POM-g-rGO, in which PIL served as surfactant to prevent aggregation of rGO sheets and binding sites for deposition of POMs. The uniform distribution of POMs on surface of rGO sheets were found to enable multiple and reversible redox reactions. Furthermore, the POM-g-rGO nanohybrids were incorporated into a flow-injection device and showed excellent electrocatalytic activity for the reduction of H_2O_2. We also examined biosensing performance for detection of glucose molecules using a flow-injection device based on POM-g-rGO nanohybrids. Chronoamperometric result demonstrated a high sensitivity, low detection limit, fast response time, and good selectivity were achievable using POM-g-rGO nanohybrids for an enzymatic electrochemical biosensor. These superior performances were attributed to multiple redox reactions of POMs, high electrical conductivity of rGO sheets, and rapid and efficient charge transfer between POMs and rGO sheets through PILs. We believe that the electrochemical performance of the devised sensor makes is an excellent and developmental cadidate for different types of electrochemical biosensors.

Acknowledgment

This work was supported by the National Research Foundation of Korea (NRF) Grant funded by the Korean Government (MSIP) (No. 2014R1A5A2010008 and No. 2015R1C1A1A02036556) and the BioNano Health-Guard Research Center funded by the Ministry of Science, ICT & Future Planning (MSIP) of Korea as Global Frontier Project (Grant number H-GUARD_2013M3A6B2078945). This research was also supported by the Ministry of Trade, Industry & Energy (MOTIE), Korea Institute for Advancement of Technology (KIAT) through the Encouragement Program for The Industries of Economic Cooperation Region.

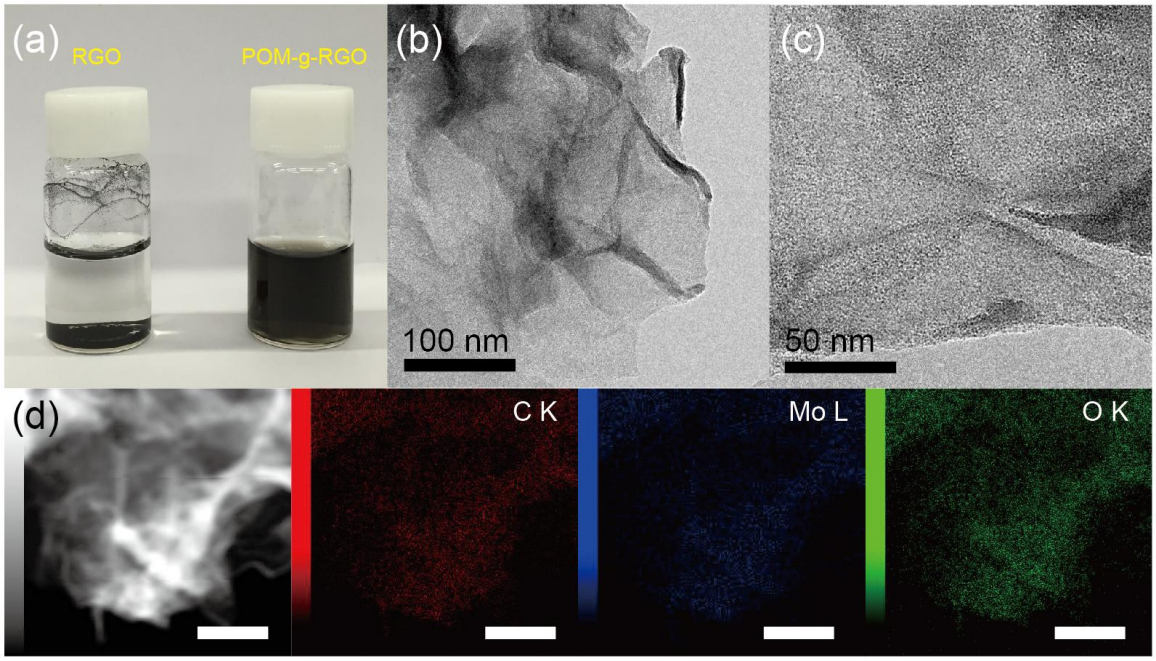

Figure 1. (a) Digital photo of rGO and POM-g-rGO dispersed in water. (b and c) TEM images of POM-g-rGO at low and high magnification, respectively. (d) HADDF TEM image and EDS elemental mapping images of POM-g-rGO (scale bar, 200 nm).

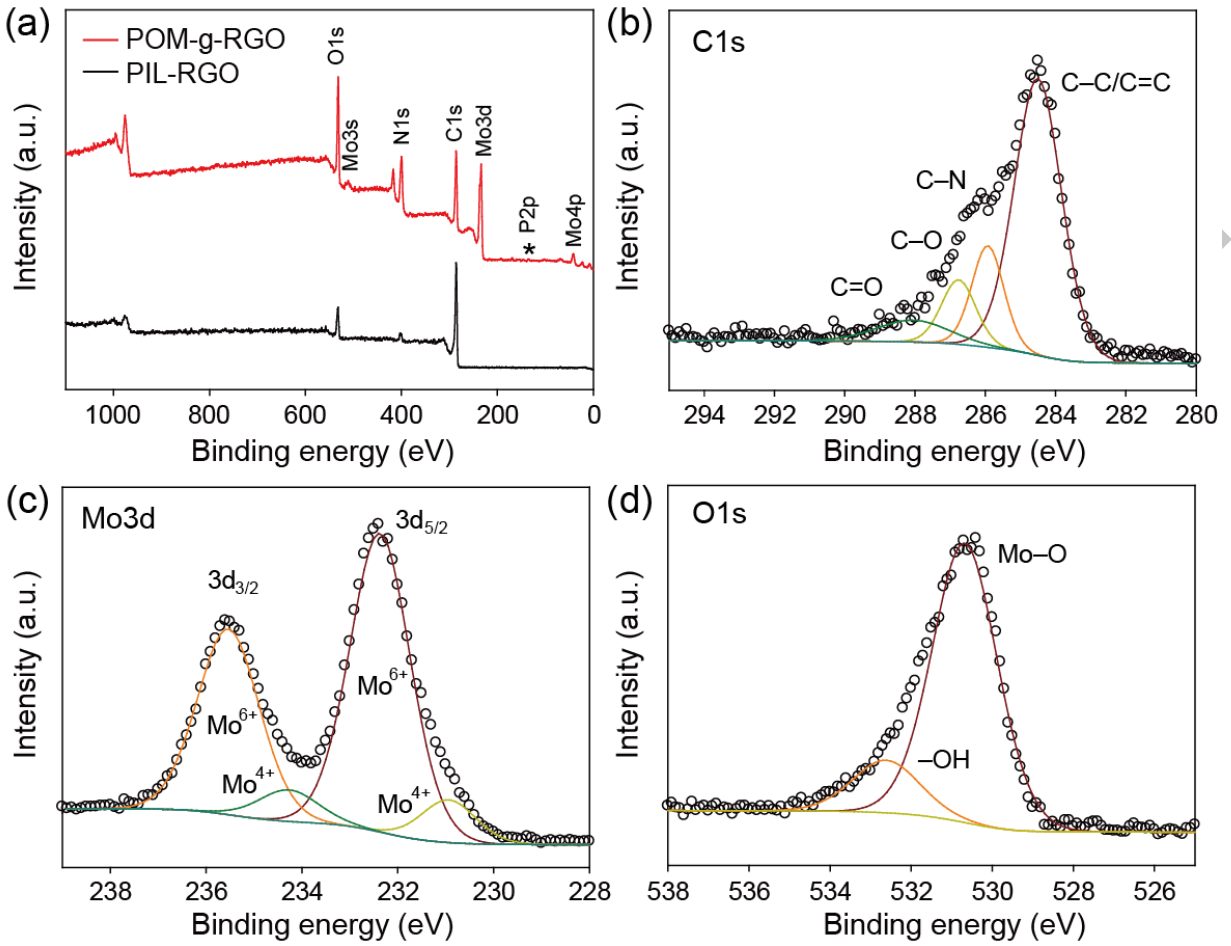

Figure 2. (a) XPS spectra of PIL-rGO and POM-g-rGO. (b) High-resolution XPS spectra of C 1s, (c) Mo 3d, and (d) O 1s for POM-g-rGO.

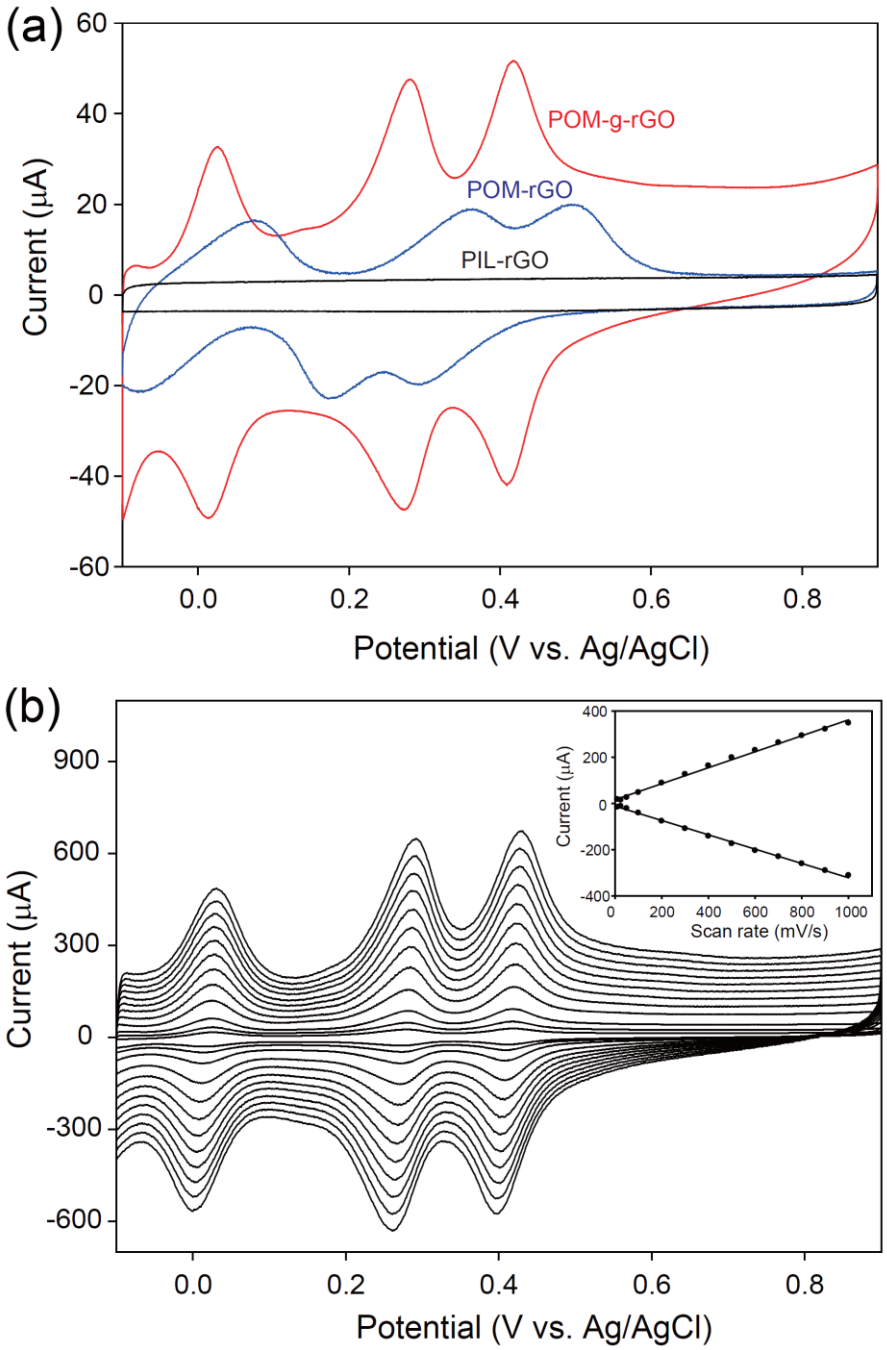

Figure 3. (a) CV curves of PIL-rGO, POM-rGO and POM-g-rGO electrode in 0.5 M H_2SO_4 at a scan rate of 50 mV/s (b) CV curves of POM-g-rGO electrode with increasing scan rates from 10 to 1000 mV/s. Inset is anodic and cathodic peak currents at a second peak position as the function of scan rate.

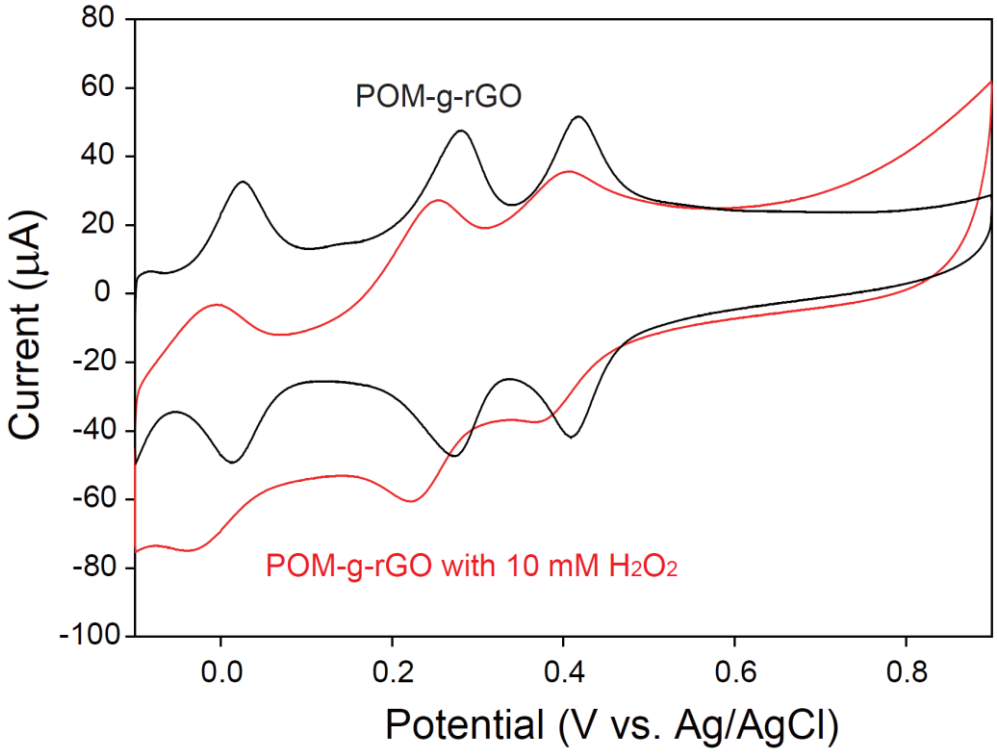

Figure 4. CV curves of POM-g-rGO electrode at scan rate of 50 mV/s in absence and presence of H_2O_2.

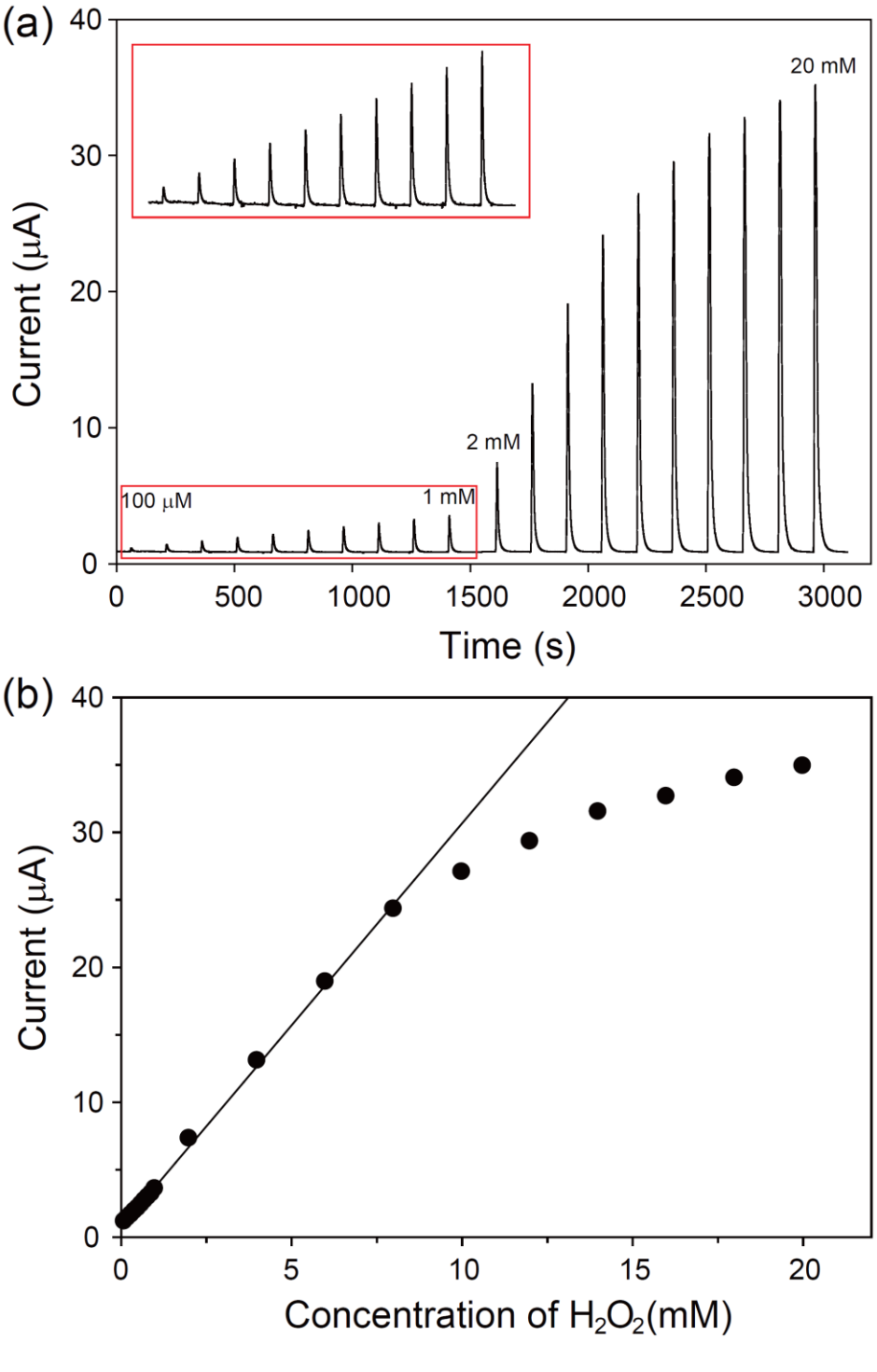

Figure 5. (a) Amperometric responses of POM-g-rGO electrode-based fluidic biosensor devices with increasing concentration of H_2O_2 ranging from 0.1 to 20 mM in the flow injection system at +0.02 V. (b) Calibration curves of the response current on the concentration of H_2O_2 at POM-g-rGO electrode-based fluidic biosensor devices.

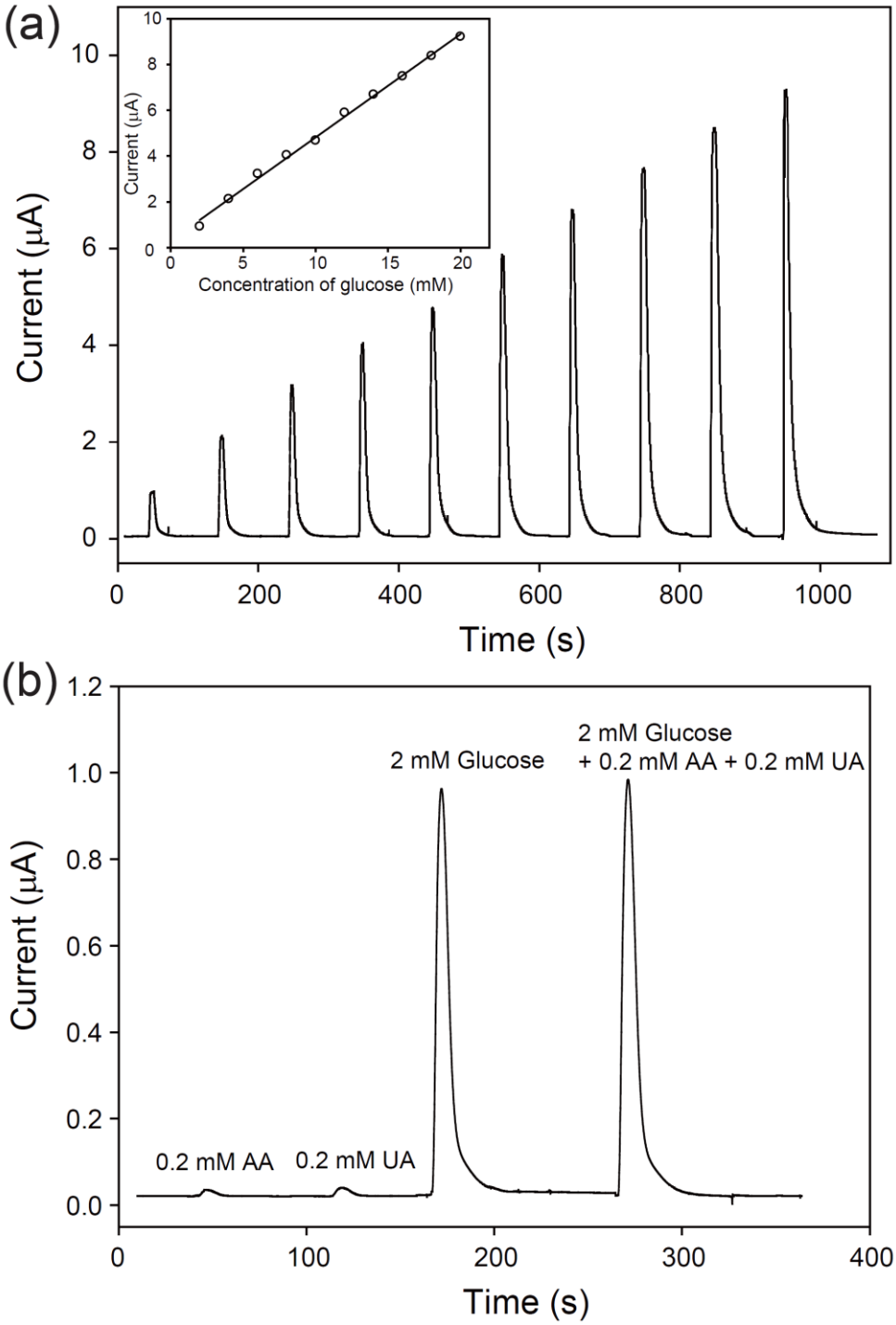

Figure 6. (a) Amperometric responses of POM-g-rGO electrode-based fluidic biosensor devices with increasing concentration of glucose ranging from 2 to 20 mM in the flow injection system at +0.02 V. Inset is calibration curves of the amperometric response to concentration of glucose. (b) Amperometric responses of interfering species on the biosensor response with subsequent addition of 0.2 mM ascorbic acid (AA), 0.2 mM uric acid (UA), 2 mM glucose, and 0.2 mM AA + 0.2 mM UA + 2 mM glucose.

REFERENCES

[1] C. Zhu, G. Yang, H. Li, D. Du, Y. Lin. Anal. Chem. 87 (2015) 230–249.

[2] R. Liu, J. Duay, S.B. Lee, Chem. Commun. 47 (2011) 1384–1404.

[3] P.T. Yin, T.-H. Kim, J.-W. Choi, K.-B. Lee, Phys. Chem. Chem. Phys. 15 (2013) 12785–12799.

[4] J.E. Johns, J.M.P. Alaboson, S. Patwardhan, C.R. Ryder, G.C. Schatz, M.C. Hersam, J. Am. Chem. Soc. 135 (2013) 18121–18125.

[5] X. Huang, X. Qi, F. Boey, H. Zhang, Chem. Soc. Rev. 41 (2012) 666–686.

[6] Z. Zanolli, R. Leghrib, A. Felten, J.-J. Pireaux, E. Llobet, J.-C. Charlier, ACS Nano 5 (2011) 4592–4599.

[7] W. Zhang, F. Li, T. Hu, S. Gan, D. Han, Q, Zhang, L. Niu, J. Mater. Chem. B 2 (2014) 3142–3148.

[8] S. Guo, D. Wen, Y. Zhai, S. Dong, E. Wang, ACS Nano 4 (2010) 3959–3968.

[9] M. Govindhan, M. Amiri, A. Chen, Biosens. Bioelectron. 66 (2015) 474–480.

[10] J. Song, L. Xu, R. Xing, Q. Li, C. Zhou, D. Liu, H. Song, Sci. Rep. 4 (2014) 7515

[11] A. Pandikumar, G.T.S. How, T.P. See, F.S. Omar, S. Jayabal, K.Z. Kamali, N. Yusoff, A. Jamil, R. Ramaraj, S.A. John, H.N. Lim, N.M. Huang, RSC Adv. 4 (2014) 63296–63323.

[12] S.K. Vashist, J.H.T. Lung, Carbon 84 (2015) 519–550.

[13] H. Gao, F. Xia, C.B. Ching, H. Duan, ACS Appl. Mater. Interfaces 3 (2011) 3049–3057.

[14] D.-L. Long, E. Burkholder, L. Cronin, Chem. Soc. Rev. 36 (2007) 105–121.

[15] M. Amman, I.-M. Mbomekalle, B. Keita, L. Nadjo, T.M. Anderson, X. Zhang, K.I. Hardcastle, C.L. Hill, J. Fransaer, J. Electroanal. Chem. 647 (2010) 97−102.

[16] B. Haghighi, H. Hamidi, L. Gorton, Electrochim. Acta 55 (2010) 4750−4757.

[17] A.Z. Ernst, L. Sun, K. Wiaderek, A. Kolary, S. Zoladek, P.J. Kulesza, J.A. Cox, Electroanalysis 19 (2007) 2103−2109.

[18] H. Ma, Y. Gu, Z. Zhang, H. Pang, S. Li, L. Kang, Electrochim. Acta 56 (2011) 7428−7432.

[19] P. Gómez-Romero, K. Cuentas-Gallegos, M. Lira-Cantú, N. Casañ-Pastor, J. Mater. Sci. 40 (2005) 1423−1428.

[20] W.S. Hummers, R.E. Offeman, J. Am. Chem. Soc. 80 (1958) 1339−1339.

[21] M. Yang, B.G. Choi, S.C. Jung, Y.-K. Han, Y.S. Huh, S.B. Lee, Adv. Funct. Mater. 24 (2014) 7301−7309.

[22] R.J. Hunter, Electrokinetics and the Zetapotential, Foundation of Colloid Science, vol. 2, Oxford University Press Inc, New York, 2011.

[23] X. An, J.C. Yu, Y. Wang, Y. Hu, X. Yu, G. Zhang, J. Mater. Chem. 22 (2012) 8525−8531.

[24] X. An, J.C. Yu, J. Tang, J. Mater. Chem. A 2 (2014) 1000−1005.

[25] P. Garrigue, M.-H. Delville, C. Kabrugère, E. Cloutet, P.J. Kulesza, J.P. Morand, A. Kuhn, Chem. Mater. 16 (2004) 2984−2986.

[26] A.J. Bard, L.R. Faulkner, Electrochemical Methods: Fundamentals and Applications, 2nd ed, John Wiley & Sons, New York, 2001.

[27] R. Liu, S. Li, X. Yu, G. Zhang, S. Zhang, J. Yao, B. Keita, L. Nadjo, L. Zhi, Small 8 (2012) 1398−1406.

[28] M. Janyasupab, C.-W. Liu, Y. Zhang, K.-W. Wang, C.-C. Liu, Sens. Actuators B: Chem. 179 (2013) 209–214.

[29] L. Zhang, Y. Ni, X. Wang, G. Zhao, Talanta 82 (2010) 1637–1641.

[30] Y. Han, J. Zheng, S. Dong, Electrochim. Acta 90 (2013) 35–43.

[31] J. Wang, Chem. Rev. 108 (2008) 814−825.

[32] G.L. Turdean, A. Curulli, I.C. Popescu, C. Rosu, G. Palleschi, Electroanalysis 14 (2002) 1550–1556.

Graphical abstract

Highly efficient electrocatalytic polyoxometalate was directly deposited on polymeric ionic liquid (PIL)-functionalized reduced grapheme oxide, leading to high electrocatalytic activity for the electrochemical detection of H_2O_2 and glucose in flow-injection biosensor device.